Peer-reviewed version available at Energies 2017, 10, 243; doi:10.3390/en10020243

Article

An Optimized Energy Management Strategy for Preheating Vehicle-Mounted Li-Ion Batteries at Subzero Temperatures

Tao Zhu [1], Haitao Min [1], Yuanbin Yu [1,*], Zhongmin Zhao [2], Tao Xu [1], Yang Chen [1] and Xinyong Li [1]

[1] State Key Laboratory of Automotive Simulation and control, Jilin University, Changchun 130022, China; zhutao14@mails.jlu.edu.cn (T.Z.); minht@jlu.edu.cn (H.M.); xutao15@mails.jlu.edu.cn (T.X.); ychen15@mails.jlu.edu.cn (Y.C.); xinyong15@mails.jlu.edu.cn (X.L.)

[2] FAW Bus and Coach Co., Ltd., Changchun 130033, China; zzm_kc@faw.com.cn

* Correspondence: yyb@jlu.edu.cn; Tel.: +86-135-0443-8449

Abstract: This paper presents an optimized energy management strategy for Li-ion power batteries used on electric vehicles (EVs) at low temperatures. Under low-temperature environments, EVs suffer a sharp driving range loss resulted from the energy and power capability reduction of the battery. Simultaneously, because of Li plating, battery degradation becomes an increasing concern as temperature drops. All these factors could greatly increase the total vehicle operation cost. Prior to battery charging and vehicle operating, preheating battery to a battery-friendly temperature is an approach to promote energy utilization and reduce total cost. Based on the proposed $LiFePO_4$ battery model, the total vehicle operation cost under certain driving cycles is quantified in the present paper. Then given a certain ambient temperature, a target temperature of preheating is optimized under the principle of minimizing total cost. As for the preheating method, a liquid heating system is also implemented on an electric bus. Simulation results show that the preheating process becomes increasingly necessary with a decreasing ambient temperature; however, the preheating demand declines as driving range grows. Vehicle tests verify that the preheating management strategy proposed in this paper is able to save total vehicle operation cost.

Keywords: electric vehicle; battery heat generation; battery degradation; vehicle operation cost; preheating target temperature; heating system

1. Introduction

Vehicle-mounted Li-ion power battery is the only energy supply system of EV, with limited electricity stored inside. Unfortunately, the performance of battery is pretty susceptible to ambient temperature. Under extreme temperature conditions, energy efficiency of battery could be rather low. Nevertheless, battery degradation is accelerated at extremely low temperatures. These factors not only greatly shorten the driving range of vehicle, but also cause a great damage to battery [1, 2]. In other words, whether the working temperature of battery is appropriate concerns not only the safety of EV but also efficiency and life of battery. Unfortunately, conventional battery thermal management system (BTMS) generally focuses on how to cool battery at high temperatures. Existing research on preheating battery at low temperatures is mainly confined to heating battery up to 0℃ before battery charging and vehicle operation, which just meets the basic requirements [3-6]. To the authors' knowledge, few published papers have illustrated: 1) what the preheating target temperature should be; 2) how to implement the preheating system on a real EV. Therefore, it is crucial to study the preheating method of battery from the perspective of energy utilization, which aims at reducing total vehicle operation cost.

Research regarding vehicle-mounted battery usually initializes with battery modeling since it has been widely used to predict the electrochemical and thermal performance of batteries [7, 8]. Generally two approaches are used in thermal modeling. The first approach involves calculating the

Peer-reviewed version available at Energies 2017, 10, 243; doi:10.3390/en10020243

heat generated in a battery based on an electrochemical model [9], and the other approach involves the use of a simplified lumped mass model based on certain assumptions [10]. However, because the former kind of models contain many dimensional and material parameters, which are difficult to obtain, and governing equations that make the computation complicated, this kind of models may not be practical for modeling the battery pack [7, 8]. On the other hand, through the second approach, Agarwal et al. [11] developed a battery model for discharging and charging power control and lifetime estimation; Ahmed et al. [12] studied the effects of temperature on internal resistances on LiMnNiO and $LiFePO_4$ batteries. Moreover, with no need to solve the complicated thermal-electrochemical equations, these proposed models directly calculate the heat generation rate from the internal resistance, improving its applicability in the BMS of electric vehicles due to its computationally efficiency.

On the other hand, battery aging has increasingly become a worrying concern when vehicles operates at subzero temperatures, resulting in battery capacity loss and impedance increment and even an internal short circuit of the cell [13]. According to Petzl et al. [14], battery current and state-of-charge (SOC) increase aggravate lithium plating and thus induce stronger degradation due to enhanced electrolyte degradation. Furthermore, evidences also showed that battery degradation was aggravated by a higher charge cut-off voltage [15]. In most cases, the degradation rate for each ageing process is strongly related to certain operating conditions such as temperature, charge and discharge rate, depth-of-discharge (DOD) and SOC region [16]. In order to explore the in-depth degradation mechanisms, differential voltage analysis and cell opening investigation have been widely used by many scholars [14]. Generally, the ageing can be categorized into three groups based on the symptoms: 1) loss of active electrode material, 2) loss of cyclable Li and 3) loss of conductivity in electrodes or electrolyte [17]. At subzero temperatures, battery degradation becomes much more severe with decreasing temperature because of the presence of the specific mechanism: the Li plating [18]. Often, battery cycle life tests are performed under accelerating conditions such as elevated temperatures, high DOD or high current rates. Based on Arrhenius Law and a large number of test data, Wang et al. [19, 20] established a semi-empirical life model to predict calendar-life loss. This model is widely adopted and further developed, but for actual vehicle usage it should be modified because the battery is subjected to complex load profiles.

Many different approaches and attaching management strategies of heating up battery have been imagined in previous studies, including forced air, liquid, heat pipe, PCM, thermoelectric and battery internal self-heating [16, 21]. However, studies showed that neither natural nor forced air convection can efficiently dissipate heat in large-scale batteries [22]. On the other hand, battery internal heating has engaged scholars' interest. Ji et al. [23] evaluated several different heating strategies from the aspects of energy consumption, heating time, heating efficiency and system cost; With sinusoidal alternating current (AC) used to achieve battery self-heating, Zhang et al. [24] pointed out that the heating rate increases with higher amplitude, lower frequency and better thermal insulation; Pesaran et al. [25] commented that compared with external heating, internal heating achieved not only a faster heating rate but also more uniform temperature distribution. However, internal heating with frequent AC may cause severe battery degradation. As for other candidates such as heat pipe and PCM, although simulation results may indicate that they were viable solutions for EVs[26], but when it comes to real application on automotive, some potential uncertainty may discourage their being used. For example, they may be faced with low heating efficiency or poor reliability in real use. In contrast, liquid heating is preferable in this paper because it is an optimal compromise among heating efficiency, device cost and system reliability.

A great variety of optimization methods have been applied successfully to various engineering problems in automotive application, achieving good performance. Optimization tools such as fuzzy logic, neural networks, heuristic rules and deterministic methods are widely used in power management, component sizing and battery thermal performance optimization of EVs. Song et al. [27] used dynamic programing (DP) to optimize the energy management in a hybrid energy storage system, but the disadvantage is that a huge computational effort has to be taken to find the optimal value. Bauer et al. [28] utilized Pontryagin's maximum principle (PMP) to solve the thermal and

energy battery management optimization, which undeniably provided a competent solution but made optimization process complicated with too many state equations involved. In the present paper, non-dominated sorting genetic algorithm Ⅱ (NSGA-Ⅱ) is used due to its convenience and efficiency.

In this paper, we manage to optimize the preheating process with answering the following questions: 1) how to establish a comprehensive battery model for automotive analysis; 2) how to quantify the cost from vehicle operation; 3) how to determine the target temperature of preheating; 4) how to arrange the preheating system on a real electric bus. The reminder of this paper is structured as follows. Section 2 presents an integrated battery model which not only describes the electro-thermal characters of battery, but also takes the variation of capacity caused by aging into consideration. Section 3 deduces the total vehicle operation cost under certain driving cycles, with total cost divided into electricity cost and battery fade cost. Section 4 determines the preheating target temperatures under different ambient temperatures by using NSGA-Ⅱ. Section 5 introduces the organization and control strategies of the preheating system. The performance of the preheating system is also assessed in this section. Section 6 conducts a road test to verify the accuracy of proposed battery model, the rationality of proposed energy management strategy and the robustness of implemented preheating system. Section 7 draws a conclusion and does some discussion.

2. Battery model consisting of electro-thermal and degradation models

2.1. Battery electrical model and parameters characterization

There are plenty of battery models proposed by other scholars. Rao et al. [29] classified battery models as 1) physical models; 2) empirical models; 3) abstract models; and 4) mixed models. Most models tend to be pretty complicated and can hardly be used in practical automotive application. With regard to battery electro-thermal analysis for automotive use, there is no need to get deeply into the complex chemical reactions inside the battery. So we adopt the *Rint* model (Figure 1) due to its simplicity and sufficient accuracy. The high-voltage battery packs used in this paper are composed of 180 cells that are connected in series. Basic parameters of the cells are shown in Table 1.

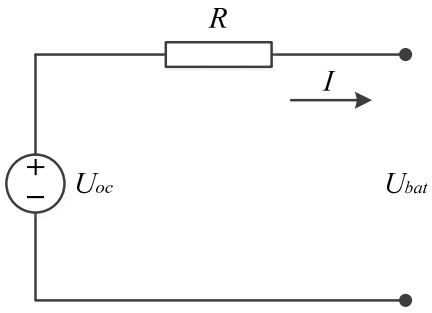

Figure 1. Equivalent circuit of battery *Rint* model

Table 1. Basic parameters of the cell

Parameters	Value or Specification
Nominal voltage	3.2V
Cathode material	LiFePO4
Anode material	Graphite
Nominal capacity	180 Ah, 576Wh
Size	282×182×71mm
Mass	5.8kg
Charge cut-off voltage	3.8V

Discharge cut-off voltage	2.8V
Operating temperature	-30~60℃
Specific heat capacity	854 J/(kg K)

Six basic parameters are characterized in the battery electrical model: 1) SOC; 2) U_{oc}-open circuit voltage (OCV); 3) R - equivalent resistance; 4) η -energy efficiency; 5) I -current; 6) U_{bat}-battery terminal voltage. These parameters are acquired by either calculation or experiments as follows:

1. *SOC* is evaluated by ampere hour integration.
2. U_{oc} is acquired through look-up SOC-OCV table and this table is obtained through experiments with battery cycler (Digatron Firing Circuits), thermostat chamber and other essential devices.
3. R is SOC and temperature dependent. It is measured by experiments using hybrid pulse power characterization (HPPC) method. The detailed procedures of measurement can be found in [30]. Test results are shown in Figure 2. According to Figure 2, the value of R under specific SOC and temperature could be acquired through look-up table.

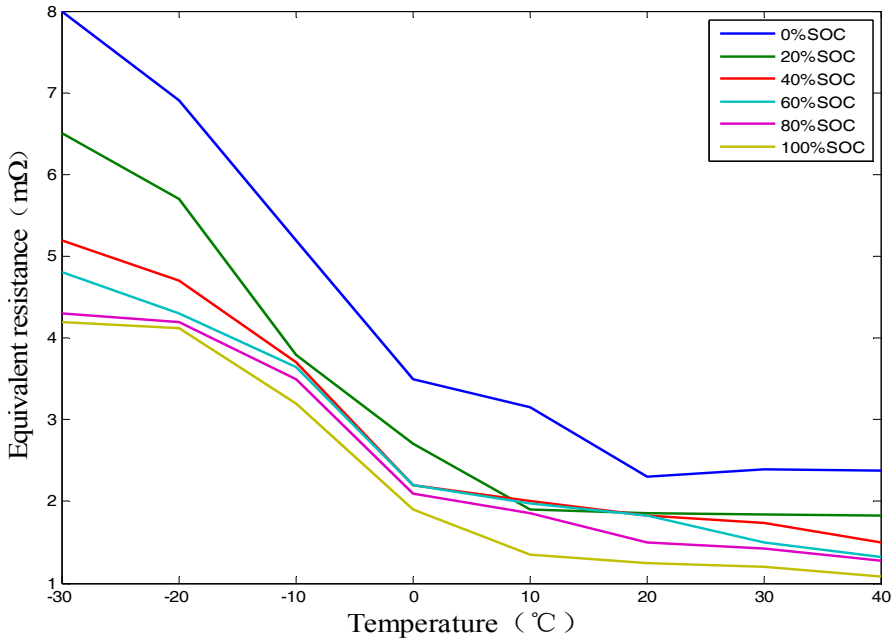

Figure 2.Cell equivalent resistance as a function of SOC and temperature

4. η is another parameter that is greatly influenced by temperature [31]. η is distinguished into discharge efficiency η_{dch} and charge efficiency η_{cha}. The expression of discharge efficiency η_{dch} is shown as follows:

$$\eta_{dch} = \frac{\int U_{dch}(t) I_{dch}(t) dt}{\int U_{dch}(t) I_{dch}(t) dt + Q_{loss}} \times 100\% \quad (1)$$

Where, U_{dch} is the terminal voltage during discharging; I_{dch} is the current during discharging; Q_{loss} is the energy loss during discharging. Figure 3 illustrates the relationship between discharge efficiency and temperature (C/2 current rate).

Preprints (www.preprints.org) | NOT PEER-REVIEWED | Posted: 6 December 2016 doi:10.20944/preprints201612.0029.v1

Peer-reviewed version available at Energies 2017, 10, 243; doi:10.3390/en10020243

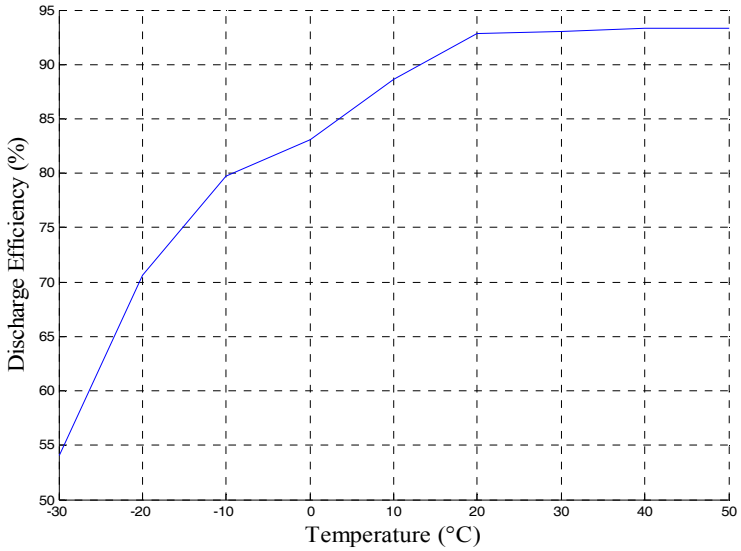

Figure 3.Discharge efficiency as a function of temperature

Similarly, charge efficiency η_{cha} can be expressed as follows:

$$\eta_{cha} = \frac{\int U_{cha}(t)I_{cha}(t)dt - Q_{loss}}{\int U_{cha}(t)I_{cha}(t)dt} \times 100\% \quad (2)$$

Where, U_{ch} is the terminal voltage during charging; I_{ch} is the current during charging; Q_{loss} is the energy loss during charging. Figure 4 illustrates the relationship between charge efficiency and temperature (C/2 current rate).

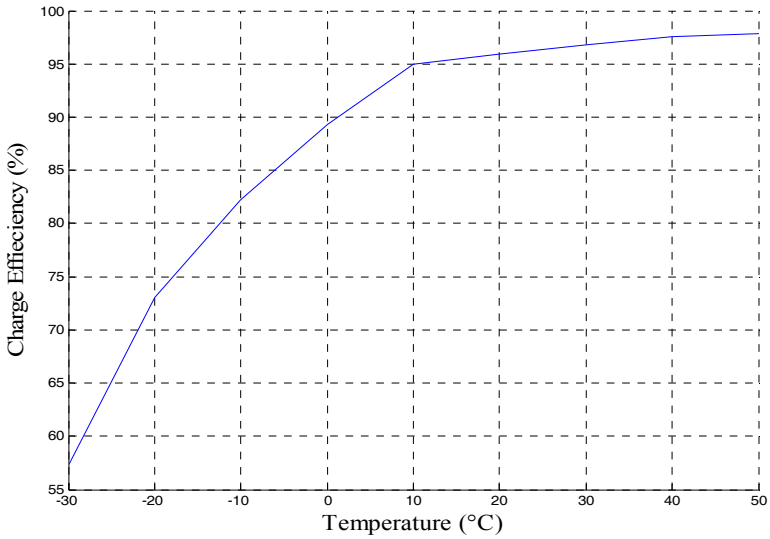

Figure 4.Charge efficiency as a function of temperature

5. I is calculated through Equation (3) [28]. P_{bat} is the battery power determined by specific driving cycles. Detailed deduction on P_{bat} is presented in Section 3.1.

$$I = \frac{U_{oc} - \sqrt{U_{oc}^2 - 4RP_{bat}}}{2R} \quad (3)$$

6. U_{bat} can be determined through Equation (4) after I is confirmed.

$$U_{bat} = U_{oc} - IR \quad (4)$$

2.2. Battery heat generation mechanism and thermal model

According to Bernadi [32], heat generated by battery during its working process could be divided into four parts: reaction heat (Q_r), side reaction heat (Q_s), polarization reaction heat (Q_p) and Joule heat (Q_j). Actually, Q_s is small enough that it could be neglected [33]. Besides, the sum of Q_p and Q_j could be replaced by the heat produced by the equivalent resistance R [34]. In summary, the total heat generated by Li-ion battery during its working process could be simplified as Equation (5) shows.

$$Q_t = Q_r + Q_p + Q_s + Q_j = Q_r + I^2Rt \quad (5)$$

Where, Q_t is the total heat generated by battery; $R = R_z + R_p$, R_z is ohmic resistance and R_p is polarization resistance; t is the time duration of charging or discharging. As for Q_r, it is endothermic during charging and exothermic during discharging. Assuming that the reversible heat for charging and discharging at the same current is equal and only differs in the sign [35], the reversible heat can be calculated using Equation (6).

$$Q_r = \frac{Q_d - Q_c}{2} \quad (6)$$

Where, Q_c and Q_d are the battery heat generated during charging and discharging respectively. According to Lin et al. [7, 8], Q_r is only approximately 6%-7% of the total heat generated. For large batteries used on electric vehicles, heat generation is mainly dominated by the Joule heat.

Temperature change of battery (ΔT) is mainly related to the heat generated by battery (Q_t, including charge and discharge) [36] and the heat dissipated from battery (Q_{dis}) [37], as shown in Equation (7).

$$\Delta T = \frac{Q_t - Q_{dis}}{m_{bat}C_p} = \frac{\int I^2Rtdt + Q_r - Q_{dis}}{m_{bat}C_p} \quad (7)$$

Where, m_{bat} is battery mass; C_p is the specific heat capacity of battery. Here the value of C_p (854 J/ (kg K)) is provided by the battery manufacturer. Actually there are two ways obtaining C_p including: 1) by measurement based on Equation (8) where the temperature variation and heat absorbed by the test sample can be experimentally acquired and 2) calculation according to Equation (9) based on the average values of the mass-weighted specific heat of each component in the battery (e.g., electrode, separator and current collector) [9]. C_p was tested by both ways and no significant difference was found between the two methods (860.3 J/ (kg K) and 858.6 J/ (kg K)). Finally the value given by the battery manufacturer was adopted because there may be unavoidable error in our own measurements.

$$Q = C_p m_{bat}(T_f - T_i) \quad (8)$$

Where, T_f and T_i are the finial temperature and initial temperature in the measurement process.

$$C_p = \frac{\sum_1^n (C_{p,i} \times \rho_i \times V_i)}{\sum_1^n (\rho_i \times V_i)} \quad (9)$$

Where, $C_{p,i}$ is the special heat capacity of component i; ρ_i is the density of component i; V_i is the volume of component i.

In Equation (7), Q_{dis} could be further expressed as follows [38]:

$$Q_{dis} = hA_{bat}(T' - T_0) \quad (10)$$

Where, h is the coefficient of heat transfer between battery and outside air. Its value was determined by experiments in Section 5.1; A_{bat} is the surface area of battery; T' is the surface temperature of battery; T_0 is the ambient temperature of battery. If the temperature of battery exceeds the upper limit (50℃), the battery cooling system will start work. But at subzero

temperatures and intermediate driving ranges, battery temperature is unlikely to exceed 50℃. Thus battery cooling is not involved in this paper.

2.3. Battery degradation model

Battery aging can be categorized into cycle aging and calendar aging [39]. Both of them could result in capacity reduction. Here it must be highlighted that calendar aging is not involved in our battery model, because the battery model is used to assist optimization over the period of vehicle operation, which means the battery is considered working all the time during this process. As for battery cycle aging evaluation, Wang [19] proposed a fitting formula (Equation 11) to describe capacity degradation ratio ($C_{loss\%}$) at different current rates and ambient temperatures.

$$C_{loss\%} = B \cdot \exp\left(\frac{-31700+370.3\times C_{rate}}{8.314T}\right)(A_h)^{0.55} \quad (11)$$

Where, B is the pre-exponential factor; C_{rate} is the current rate; T is the absolute temperature; A_h is the Ah-throughput, which is expressed as A_h= (cycle number) × (DOD) × (full battery capacity). The disadvantage of this formula is that it cannot describe battery degradation at subzero temperatures accurately [18].Based on Equation (11), Song [27] proposed a modified formula (Equation 12) to predict capacity loss of $LiFePO_4$ battery, which proved to be accurate over a wide temperature range, especially at subzero temperatures.

$$C_{loss\%} = 0.0032 \cdot \exp\left(\frac{-15162+1516\times C_{rate}}{8.314\times(|285.75-T|+265)}\right)(A_h)^{0.849} \quad (12)$$

As aforementioned, vehicle-mounted battery is subject to specific driving cycles. The current rate and temperature of battery keeps changing during vehicle operation. For simulation purpose, some alteration on Equation (12) is needed. Its derivative can be deduced as:

$$\dot{C}_{loss\%} = \frac{\Delta C_{loss\%}}{\Delta A_h} = 0.0032 \cdot 0.849 \cdot \exp\left(\frac{-15162+1516\times C_{rate}}{8.314\times(|285.75-T|+265)}\right)(A_h)^{0.849-1} \quad (13)$$

Where, $\Delta C_{loss\%}$ and ΔA_h are the increment of capacity degradation ratio and Ah-throughput respectively, and ΔA_h can be obtained by ampere hour integration. By discretization, Equation 13 can be further expressed as:

$$\Delta C_{loss\%,i} = 2.7168 \cdot 10^{-3} \cdot \exp\left(\frac{-15162+1516\times C_{rate}}{8.314\times(|285.75-T|+265)}\right)(A_{h,i-1})^{-0.151} \cdot \Delta A_{h,i-1} \quad (14)$$

The total capacity degradation ratio after simulation process can be expressed as:

$$C_{loss\%} = \sum_{i=1}^{n}(\Delta C_{loss\%,i}) \quad (15)$$

Equation (14) and (15) are adopted as battery aging model in simulation process.

2.4. Battery coupling model composed of electro-thermal and degradation models

Through the electro model, battery SOC could be acquired based on ampere hour integration. However, Section 2.3 indicates that battery aging could lead to non-negligible capacity loss. Thus, this factor is supposed to be coupled into the electro-thermal model to make the entire battery model more accurate. Figure 5 shows the structure of coupled battery model.

Preprints (www.preprints.org) | NOT PEER-REVIEWED | Posted: 6 December 2016 doi:10.20944/preprints201612.0029.v1

Peer-reviewed version available at Energies 2017, 10, 243; doi:10.3390/en10020243

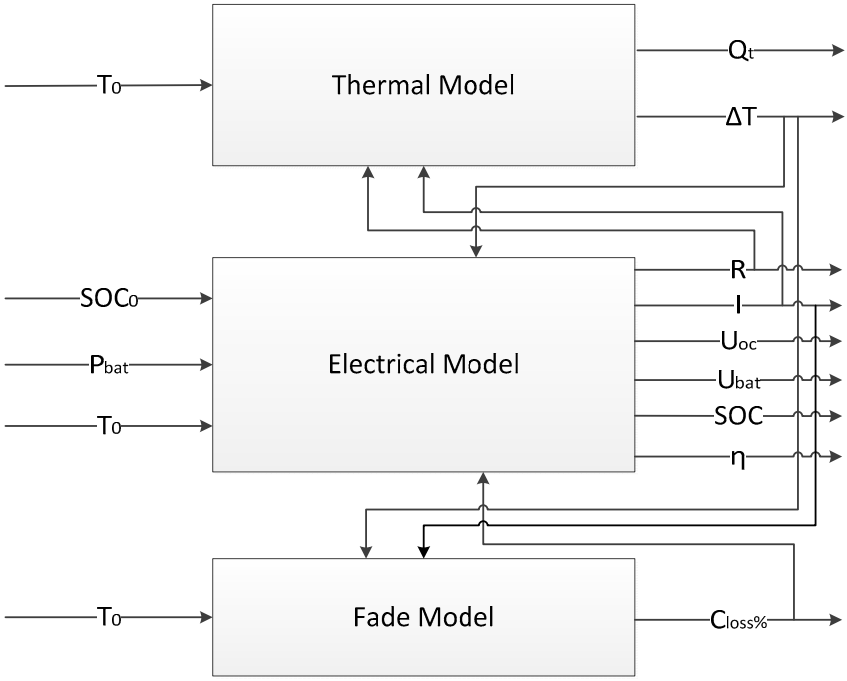

Figure 5. Coupled battery model

After degradation was taken into consideration, the modified formula for SOC evaluation should be:

$$SOC=SOC_0-\int\frac{I}{C_0\cdot(1-C_{loss\%})}dt \quad (16)$$

Where, SOC_0 and C_0 are the initial SOC and the initial capacity respectively. So far, the entire battery model consisting of electro-thermal and fade models has been established.

3. Deduction on total vehicle operation cost

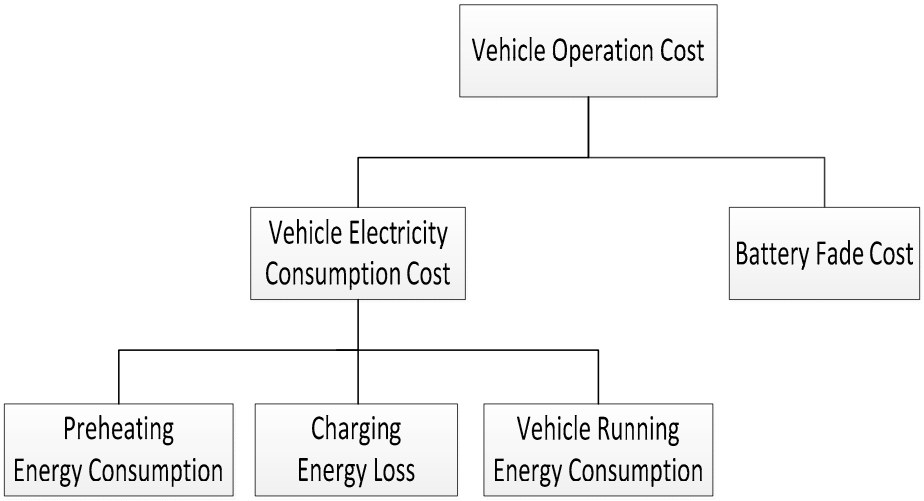

Figure 6.Components of vehicle operation cost

It is assumed that the vehicle is preheated to target temperature firstly, and then charged. After charging, vehicle starts to run. During the entire process, vehicle operation cost C_{sum} is considered as the sum of vehicle electricity consumption cost C_{ele} and battery fade cost C_{fade} (Figure 6). Table 2 shows the basic parameters of the electric city bus.

Preprints (www.preprints.org) | NOT PEER-REVIEWED | Posted: 6 December 2016 doi:10.20944/preprints201612.0029.v1

Peer-reviewed version available at Energies 2017, 10, 243; doi:10.3390/en10020243

Table 2. Basic parameters of the electric bus

Parameters	Value
Vehicle mass, m_{veh}	13946 kg
Vehicle size	11983 mm×2250 mm×3720 mm
Final drive ratio, i_o	3.7
Gearbox ratio, i_g	3.757/1.969
Wheel radius, r	0.506 m
Gravity acceleration, g	9.8 $m\ s^{-2}$
Rolling resistance coefficient, f	0.013
Air drag coefficient, C_D	0.7
Front area, A_{veh}	9.5 m^2
Motor efficiency, η_{motor}	85%
Transmission efficiency, η_T	88%
Motor inverter efficiency η_i	90%

3.1. Vehicle electricity consumption cost

Vehicle electricity consumption (Q_{ele}) originally comes from the charging pile, so Q_{ele} could be further divided into three parts (Equation 17): energy consumption of preheating (Q_{ph}), energy loss of charging (Q_{cha}) and energy consumption of vehicle running during driving cycles (Q_{cyc}). It should be highlighted here that Q_{cha} is the energy lost in charging process, rather than the energy consumption during whole charging process. In other words, Q_{cha} is a part of the energy consumption of charging, while the other part is transmitted into chemical energy and stored in battery. Then the energy stored in battery is partially consumed during driving cycles, turned into Q_{cyc}.

$$Q_{ele} = Q_{ph} + Q_{cha} + Q_{cyc} \tag{17}$$

Q_{ph} is mainly related to preheating target temperature (T_1), ambient temperature (T_0) and preheating efficiency (η_{ph}), as shown in Equation (18).

$$Q_{ph} = m_{bat}C_p(T_1 - T_0)/\eta_{ph} \tag{18}$$

Q_{cha} is mainly related to charging efficiency (Q_{cha}), charging voltage (U_{cha}), charging current (I_{cha}) and charging time (t_1~t_2), as shown in Equation (19).

$$Q_{cha} = \int_{t_1}^{t_2} U_{cha}I_{cha}(1 - \eta_{cha})\,dt \tag{19}$$

Q_{cyc} is mainly related to battery power (P_{bat}), as shown in Equation (20).

$$Q_{cyc} = \int_{t_2}^{t_3} P_{bat}dt \tag{20}$$

P_{bat} varies with vehicle speed which is determined by specific driving cycles. It should be noted that P_{bat} for driving and braking differs in the sign. When vehicle is driving, the battery will provide power to drive the motor; while vehicle is barking, since braking energy recovery is involved, the motor will charger the battery instead. So P_{bat} and Q_{cyc} should be solved in terms of driving and braking respectively:

1. Driving:

When vehicle is driving, the battery power ($P_{bat,drv}$) could be expressed as follows:

$$P_{bat,drv} = \frac{P_{veh}}{\eta_T \times \eta_{motor} \times \eta_i \times \eta_{dch}} \tag{21}$$

Where, P_{veh} is the power demand of vehicle and it could be further expressed as follows [40]:

$$P_{veh} = \frac{m_{veh}\,gf}{3600}u + \frac{m_{veh}\,gi}{3600}u + \frac{C_D A_{veh}}{76140}u^3 + \frac{\delta m_{veh}}{3600}u\frac{du}{dt} \tag{22}$$

Where, u is vehicle speed; i is the gradient of roads; δ is the correction coefficient of rotating mass. $P_{bat,drv}$ could be acquired in combination with (21) and (22). The energy consumption of driving cycles when vehicle is driving ($Q_{cyc,drv}$) could be accessed in combination with (20) (21) and (22), as Equation (23) shows.

$$Q_{cyc,drv} = \frac{1}{0.64}\int \frac{\frac{Gf}{3600}u+\frac{Gi}{3600}u+\frac{C_D A_{bat} u^3}{76140}+\frac{\delta m_{veh} u}{3600}\frac{du}{dt}}{\eta_{dch}}dt \quad (23)$$

2. Braking:

Braking energy recovery of driving wheels is involved when vehicle is braking. At this time, the motor would charge the battery, and the braking force of motor (F_{motor}) is related to braking intensity (z). According to braking force distribution and ECE regulations [40], when:

$$F_{motor} = \begin{cases} m_{veh} zg, & z \le 0.1 \\ \lambda F_{mec}, & 0.1 < z \le 0.5 \\ F_b - F_{rear}, & 0.5 < z \le 0.7 \\ 0, & z > 0.7 \end{cases} \quad (24)$$

Where, F_{mec} is mechanical braking force; λ is the coefficient between F_{motor} and F_{mec}; F_b is the total braking force of vehicle; F_{rear} is the braking force of rear axle.

In addition, the relationship between the regenerative power of motor (P_{motor}) and F_{motor} could be expressed as shown below:

$$P_{motor} = \frac{F_{motor} n r}{9549 i_o i_g \eta_T} \quad (25)$$

Where, n is the rotational speed of motor. Then when vehicle is barking, the battery power ($P_{bat,bra}$) could be expressed as:

$$P_{bat,bra} = P_{motor} \cdot \eta_{motor} \cdot \eta_i \cdot \eta_{cha} \quad (26)$$

The energy consumption of driving cycles when vehicle is braking ($Q_{cyc,bra}$) could be accessed in combination with (20) (24) (25) and (26), as Equation (27) shows.

$$Q_{cyc,bra} = \int \frac{F_{motor} \cdot n \cdot r \cdot \eta_{motor} \cdot \eta_i \cdot \eta_{cha}}{9549 i_o i_g \eta_T} dt \quad (27)$$

In summary, the energy consumption of the whole driving cycles, including both driving and braking, could be accessed as Equation (28) shows.

$$Q_{cyc} = Q_{cyc,drv} - Q_{cyc,bra} = \int \frac{\frac{Gf}{3600}u+\frac{Gi}{3600}u+\frac{C_D A_{bat} u^3}{76140}+\frac{\delta m_{veh} u}{3600}\frac{du}{dt}}{0.64 \cdot \eta_{dch}} dt - \int \frac{F_{motor} \cdot n \cdot r \cdot \eta_{motor} \cdot \eta_i \cdot \eta_{cha}}{9549 i_o i_g \eta_T} dt \quad (28)$$

After Q_{cyc} is solved, Q_{ele} is consequently determined. The electricity cost is assumed to be 0.1$/kWh, according to a report by the U.S. Energy Information Administration [27]. So the vehicle electricity consumption cost (C_{ele}) is:

$$C_{ele} = Q_{ele} \cdot 0.1\$/kWh \quad (29)$$

3.2. Battery fade cost

According to automotive standards, 80% capacity retention generally indicates the end of life (EOL) [14]. Besides, the price of the LiFePO4 battery we used is equal to 1200 $/kWh. The capacity of the whole battery is 103.68kWh. So the battery fade cost (C_{fade}) is:

$$C_{fade} = \frac{C_{loss\%}}{1-80\%} \cdot 1200 \cdot 103.68\ \$ \quad (30)$$

4. Determination of preheating target temperatures

Preheating may improve battery energy efficiency and retard aging at subzero temperatures, consequently save vehicle operation cost. However, preheating itself costs a large amount of energy; also if battery was heated to an excessively high temperature, its degradation could be far more severe. As a consequence, a near-optimal preheating target temperature is needed so that the total vehicle operation cost could be least. According to analysis in above sections, if given certain driving cycles, the total operation cost at any ambient temperature is able to be worked out. A 310s-5km driving cycle is used in this paper, which is shown in Figure 7. This driving cycle is circulated in the case of long driving ranges. Under the principle of minimizing total vehicle operation cost, NSGA-Ⅱ [41] is introduced into the simulation process to acquire the preheating target temperatures at different ambient temperatures and driving ranges. NSGA-Ⅱ is usually used to solve multi-objective optimization. For single-objective global optimization, it also shows a rapid processing capacity with low computational complexity, and high reliability with elitist strategy.

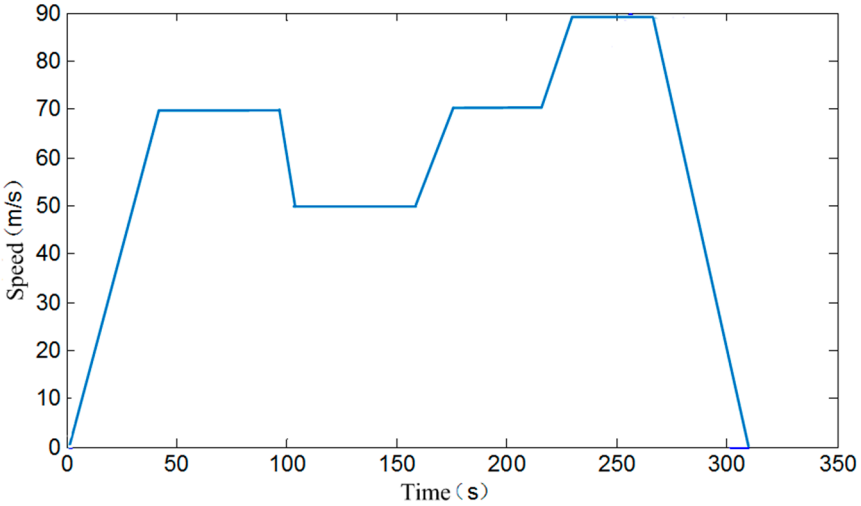

Figure 7.Driving cycle of city bus in Changchun

In the present paper, the optimization objective is vehicle operation cost C_{sum} and optimization variable is preheating target temperature T_1 (1°C interval, 20°C upper limit). Ambient temperature T_0 and driving range L are set as different constants in each simulation process. So the optimization problem could be expressed as:

$$\begin{cases} \min \mathrm{J} = \min\{\mathrm{C_{sum}}(\mathrm{T_1})\} \\ \mathrm{T_0} \le \mathrm{T_1} \le 20^\circ\ \mathrm{C} \end{cases} \tag{31}$$

For example, assuming that T_0 is -10°C; L is 20 km; SOC_0 is 20% and then battery is fully charged to 100% SOC; after being charged, the vehicle operates according to Figure 7. Optimization results given by NSGA-Ⅱ indicates that the optimal preheating target temperature is 2°C, and corresponding vehicle operation cost is 88.74 USD (electricity consumption cost and battery fade cost are 4.36 USD and 84.38 USD respectively). It means that if battery was preheated to 2°C before battery charging and vehicle operating, the vehicle could achieve least cost. In order to further validate this, the electricity consumption, battery fade ratio and vehicle operation cost at different preheating target temperatures are calculated and the results are shown in Figure 8. It is clearly shown in Figure 8 (a) that electricity consumption grows with increasing preheating temperatures, which means although preheating could improve energy efficiency of battery, but the preheating process would consume far more electricity than it can save inside the battery. Figure 8 (b) shows that there is an optimal preheating temperature at which the battery degradation could be at least. This is because at both too high and too low temperatures, battery always suffers severe degradation. So in terms of reducing capacity loss, battery would better work at intermediate temperatures. Figure 8 (c) gives the optimal preheating target temperatures from the point of

Preprints (www.preprints.org) | NOT PEER-REVIEWED | Posted: 6 December 2016 doi:10.20944/preprints201612.0029.v1

Peer-reviewed version available at Energies 2017, 10, 243; doi:10.3390/en10020243

comprehensive consideration of electricity consumption and battery fade. Comprehensive comparation of these three figures, it can also be seen that the determination of the optimal preheating target temperature mainly depends on the factor of battery fade, rather than electricty consumption.

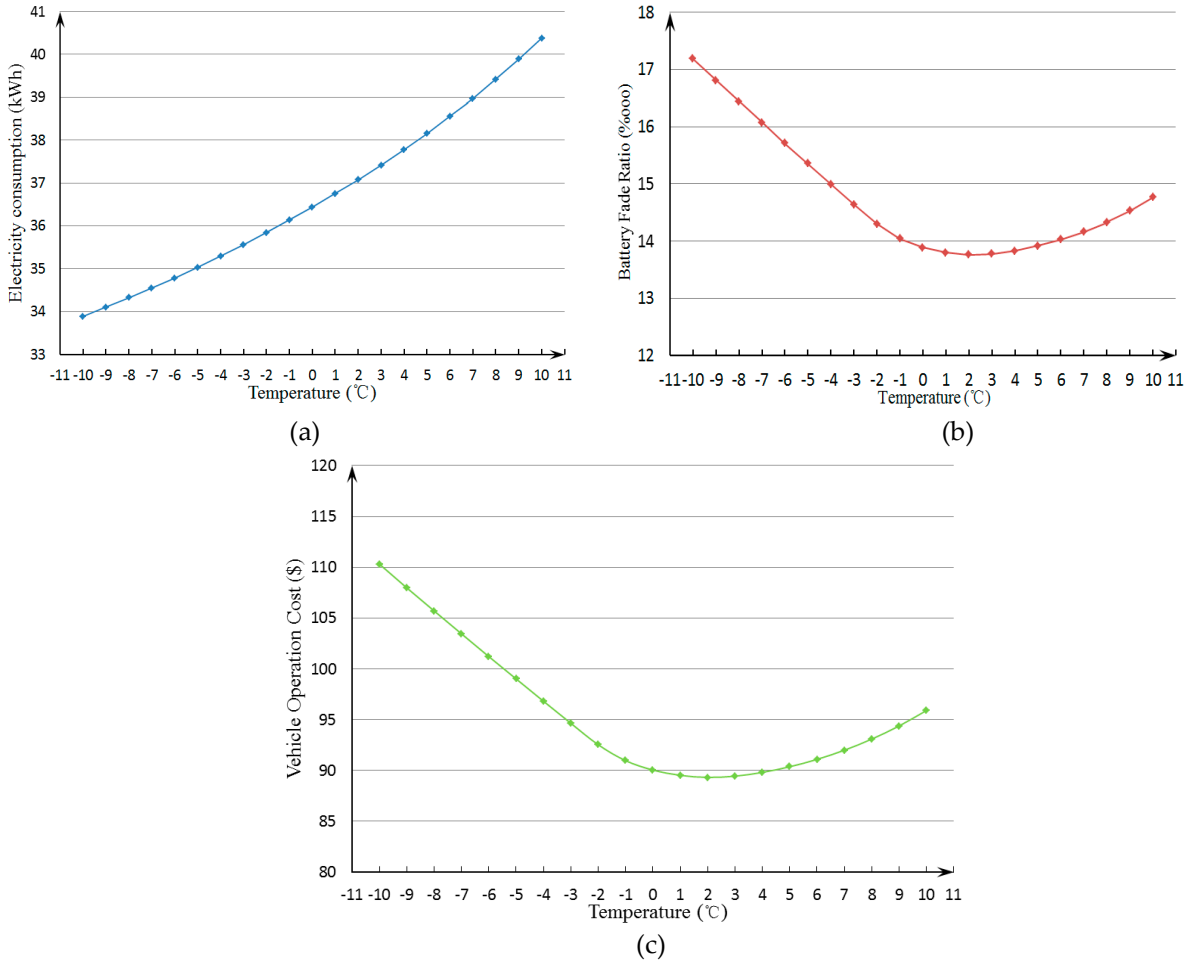

Figure 8. When ambient temperature T_0 is -10°C, driving range L is 20 km, SOC range of charging is 20%~80%, and vehicle is preheated to different temperatures, after vehicle operation, corresponding (a) electricity consumption, (b) battery fade ratio and (c) vehicle operation cost

By using NSGA-Ⅱ, every optimal preheating target temperature at different ambient temperatures and driving ranges are worked out. Based on these data, Figure 9 is plotted to present the optimal relationship between driving ranges, ambient temperatures and preheating target temperatures.

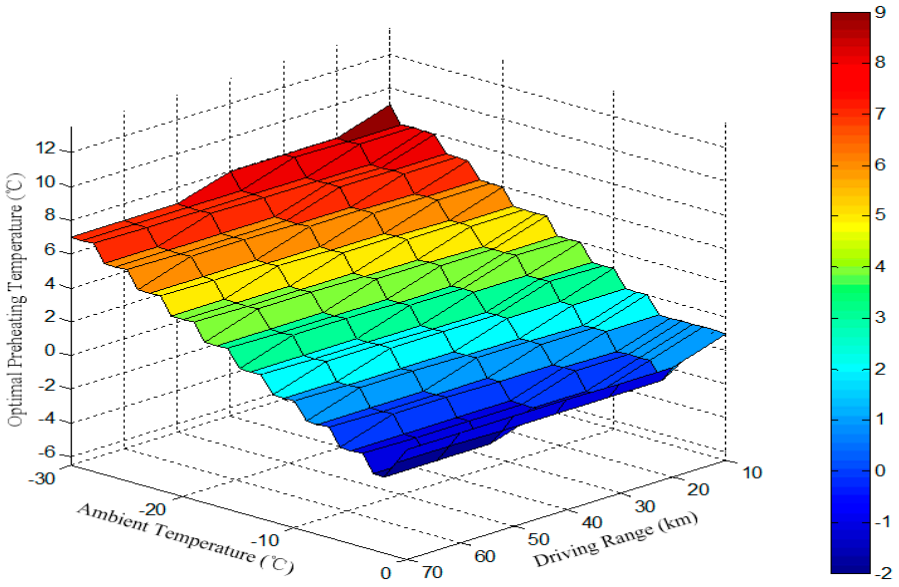

Figure 9. Optimal preheating target temperatures at different ambient temperatures and driving ranges

It is considerably noticeable that as ambient temperature gets lower, the optimal preheating target temperature gets higher. This is because battery needs to escape the low temperatures at which degradation could be rather serious. At this point, we get a similar conclusion with Song et al. [27]. But interestingly, simulation results indicate that as driving range gets longer, the optimal preheating target temperature should become lower, which means smaller preheating demand are needed for long-distance running. This is different from Song's conclusion. We think this is because in Ref. [27], battery internal heat generation (IHG) is neglected. But for large battery used in electric bus, IHG could be large, especially for long-distance driving. This IHG could result in considerable temperature rise, leading the battery temperature to a high range, where the battery degradation becomes severer. So in this case, lower preheating target temperature is needed to avoid leading battery to excessively high temperatures during vehicle operation.

5. Implementation and control of preheating system

5.1. Selection and implementation of preheating system

Liquid heating method is selected to achieve preheating battery. Compared to other heating methods, liquid provides better thermal conductivity and higher convective heat transfer rate [23]. Besides, another important reason is that there is a ready-made liquid cooling system on the electric bus used for cooling battery in summer. From the perspectives of cost saving and minimum modification, it is advisable to adopt this way of preheating because only little change needs to be made on the basis of original cooling system [42]. Figure 10 shows the cell with liquid cycle inside. Figure 11 shows the structure of modified preheating system. Compared to original cooling system, the modified preheating system added three PTC heaters and an external electric socket; disconnected the compressor, evaporators and condensers. The electric socket is used to connect a heating plug linking to the charging pile, so the charging pile could supply power to the heaters. Each heater, with a max power of 8kW, is used to heat the heating medium (glycol-water mixture 2:3) in the cycle. The water cycle is driven by the pump, flowing and heating the battery. The electric bus and actual layout of heating pipes in battery box is shown in Figure 12.

Peer-reviewed version available at Energies 2017, 10, 243; doi:10.3390/en10020243

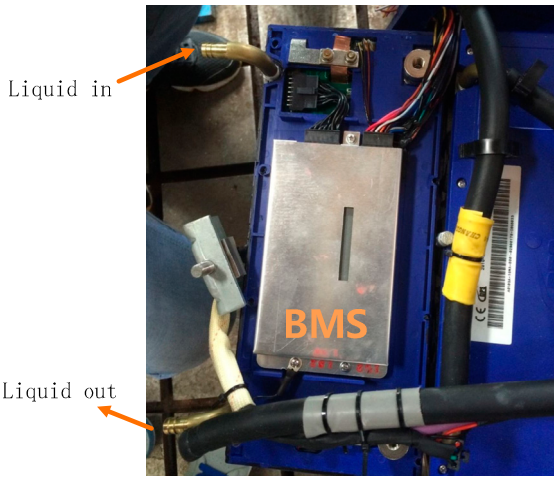

Figure 10. Cell with liquid cycle inside

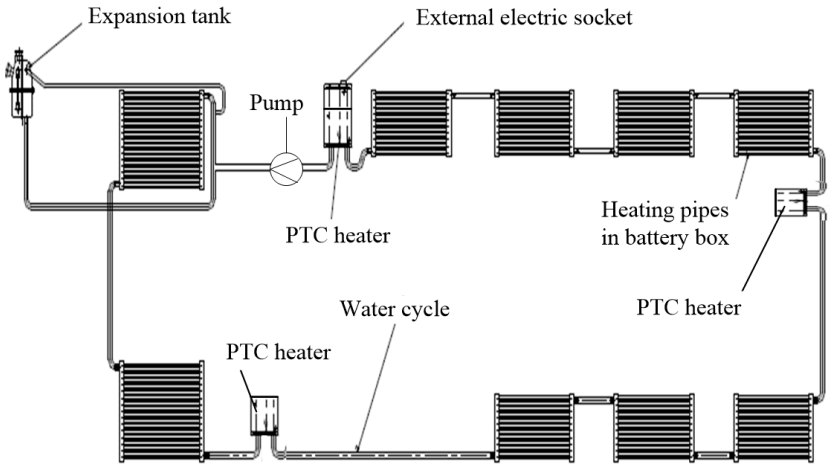

Figure 11. Structure of preheating system

Figure 12. Electric bus and actual layout of heating pipes in battery box

As aforementioned in Section 2.2, the value of heat transfer coefficient h has a significant influence on temperature rising of battery. In other words, if the value of h was too large, the battery itself could dissipate too much heat, which leads to poor performance of preheating system. As a consequence, we attached a thermal insulation blanket (made by asbestos) to the battery box.

Experiments were conducted to measure corresponding heat transfer coefficient. Since the space of a thermostat chamber is not able to contain a whole battery pack, experiments for a cell were carried out instead. Firstly the cell was covered by the thermal insulation blanket and stored under ambient temperature (-10°C) for a quite long time, so its temperature could be considered equal to -10°C. Then the cell was put into a thermostat chamber (held at 30 °C). The cell temperatures were measured during the process using one thermocouple attached to the core of the cell (Figure 13). According to Equation (32), the value of h could be calibrated from the heating curve of the cell. After several repeated experiments (different temperature ranges were set), the average value 15.86 $w/(m^2K)$ was adopted for h and this value was used in Section 4 for simulation.

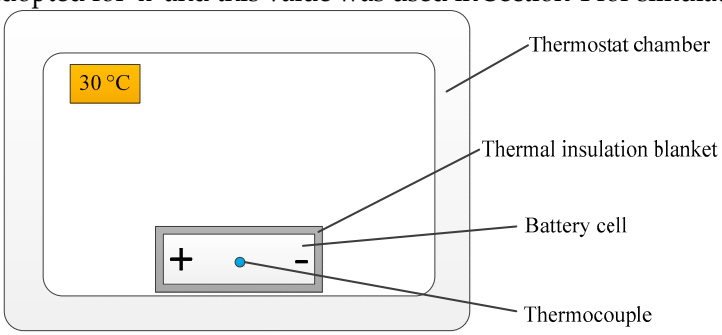

Figure 13. Experimental setup for measuring heat transfer coefficient h

$$m_{cell} C_p \frac{dT}{dt} = -h\, A_{cell}(T - T_c) \quad (32)$$

Where, m_{cell} is cell mass; A_{cell} is the surface area of cell; T_c is temperature of thermostat chamber.

5.2. Control strategy for coordinating the process of preheating and charging

The workflow of corresponding control strategy is shown in Figure 14. Although preheating process is prior to charging process, preheating will only start with both preheating plug and charging plug (Figure 15) inserted into corresponding sockets on battery. When both plugs are connected to their sockets, the low-voltage relay of battery will be closed by the 24V electric from the charging pile. As a consequence, battery management system (BMS) will power on [43]. Vehicle control unit (VCU) also needs to be waked up because it is supposed to control the preheating process. VCU and BMS will exchange information with the charging pile through CAN communications. The purpose of this information interaction is to check whether the status of VCU and battery is healthy or not. If not, neither preheating nor charging is permitted so as to avoid undesirable dangers. After detection is passed, VCU will judge whether there is the need for preheating based on ambient temperature and given driving range. If the battery does need heating, VCU will close high-voltage relay 1 (for preheating) and then charging pile could supply power to the PTC heaters. The heaters will keep working until the battery reaches the target temperature. At that time, high-voltage relay 1 will be disconnected and preheating process is completed.

After VCU detected that high-voltage relay 1 is reliably disconnected, the high-voltage relay 2 (for charging) will be closed by BMS, which means that battery enters charging mode. When charging is finished, the high-voltage relay 2 will be disconnected by BMS. When both plugs are pulled out, BMS power off. Finally the electric bus is ready to drive.

Preprints (www.preprints.org) | NOT PEER-REVIEWED | Posted: 6 December 2016 doi:10.20944/preprints201612.0029.v1

Peer-reviewed version available at Energies 2017, 10, 243; doi:10.3390/en10020243

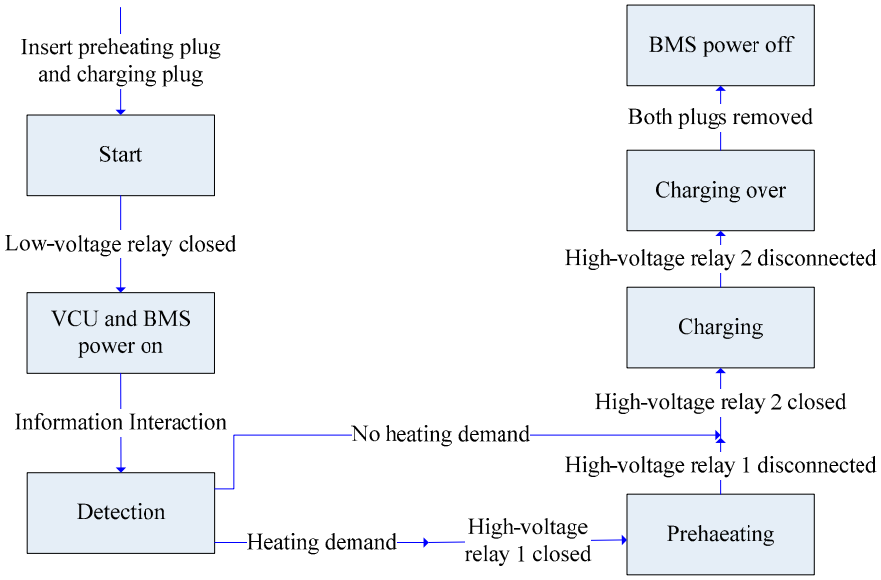

Figure 14. The control strategy for coordinating the process of preheating and charging

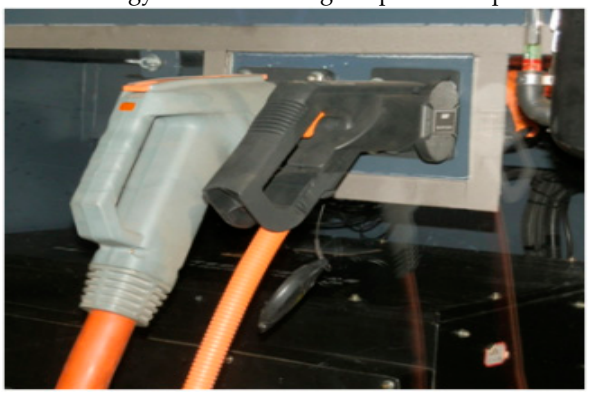

Figure 15. Charging plug (left) and heating plug (right)

5.3. Performance of the preheating system

The performance of the preheating system is assessed through five items:

1. Power source: The preheating system is powered by charging piles. Compared with battery self-heating whose power supply is battery itself, this preheating system could save the energy inside battery, which prolongs vehicle's driving range indirectly;

2. System cost: Three PTC heaters, an external electric socket and several relays were added on the basis of original cooling system, so it is very cost-saving;

3. Temperature uniformity: To some extent, temperature imbalance among different cells is unavoidable because the water cycle is too long. However, exactly because of this reason, three distributive PTC heaters were arranged at different positions in the water cycle (Figure 11) to reverse this trend. According to the information collected by BMS, if these three heaters were given same power, the biggest temperature difference among different cells is 3.1°C.

4. System efficiency: Here the heating efficiency (η_{ph}) is defined as:

$$\eta_{ph} = \frac{m_{bat} C_p \Delta T}{\int U_{cp} I_{cp} dt} \quad (33)$$

Where, U_{cp} and I_{cp} are the voltage and current of the charging pile during preheating process respectively. The heating efficiency was calculated with ambient temperature being -10°C and the results showed an average efficiency of 78%.

5. Heating time: The heating time was tested with ambient temperature being -10°C, target temperature being 2°C and power of each heater being 8 kW (max power). The tested preheating time is 1157s. Compared with other preheating method such as self-heating, this preheating time is

much longer. As a consequence, the utilization of the electric bus should be scheduled carefully. The long heating time is a serious disadvantage of liquid heating.

6. Vehicle test

Vehicle tests were conducted at: 1) ambient temperature of -10°C, which was the outdoor temperature during our tests; 2) driving range of 20km. Long-distance driving was not preferable in case of accumulative errors; 3) 20% SOC before charging and 100% SOC after charging. This is because it is often the case that SOC window for vehicle-mounted battery is 20%~100%.

Two tests were conducted with different preheating strategies:

1. Battery without preheating. Keep battery SOC at 20% through charging or discharging, and then cool battery to ambient temperature. After this, fully charge battery without preheating. Then drive the electric bus for 20km in accordance with the driving cycles in Figure 7.

2. Battery heated to 2°C (optimal target temperature given by simulation). Keep SOC of battery at 20% through charging or discharging, and then cool battery to ambient temperature. After this, preheat battery to 20°C before charging. Then fully charge battery and drive the electric bus for 20km in accordance with the driving cycles in Figure 7.

During charging process, the conventional CC-CV (first constant current, and then constant voltage) was not utilized in the tests. Instead, a two-stage constant current charging method was used [44]. This is because a pack with cells in series is not suitable for constant voltage charging. During vehicle operation process, test data such as battery temperature were collected by computers, which are linked to BMS and VCU through CANoe, as Figure 16 shows.

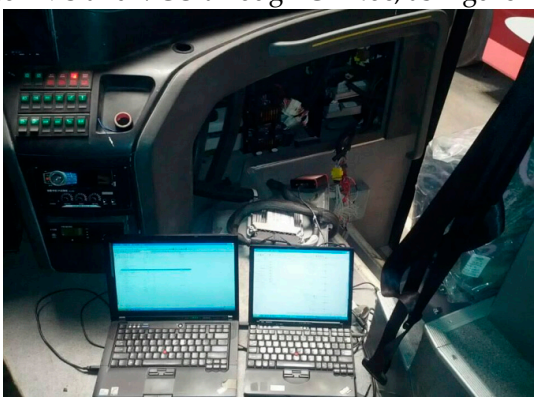

Figure 16. Data collection in vehicle tests

Test results and comparison with simulation results are shown in Table 3. It is clearly shown in this table that if battery was heated to 2°C before charging, after vehicle operation, nearly 50 $ could be saved compared to that without preheating. It is a considerable cost saving, which proves the necessity of the preheating management strategy. Preheating made more SOC remain in battery after driving cycles, which was because higher energy efficiency leads to lower energy consumption in charging process and driving cycles. What is more, after being heated, battery capacity degradation became less severe, which is the uppermost contribution of preheating to reducing total vehicle operation cost. Besides, no significant difference between test and simulation values was found. The difference for items such as SOC may be reasonable, because in real vehicle operation many accessories on vehicle also consumed electricity, which resulted in a lower SOC value compared with simulation value.

Preprints (www.preprints.org) | NOT PEER-REVIEWED | Posted: 6 December 2016 doi:10.20944/preprints201612.0029.v1

Peer-reviewed version available at Energies 2017, 10, 243; doi:10.3390/en10020243

Table 3. Vehicle test results

Test items	Test 1 Battery without heating (Test / Simulation)	Test 2 Battery heated to 2℃ (Test / Simulation)
Initial SOC	20 / 20 %	20 / 20 %
SOC after charging	100 / 100 %	100 / 100 %
SOC after driving	72.07 / 74.75 %	73.71 / 75.75 %
Energy consumption of preheating (Q_{ph})	0 / 0	14.38 / 13.29 kWh
Energy loss of charging (Q_{cha})	12.67 /12.55 kWh	5.31 /5.24 kWh
Energy consumption of driving cycles (Q_{cyc})	28.96 / 26.18 kWh	27.26 / 25.14 kWh
Battery fade ratio ($C_{loss\%}$)	0.023 / 0.022 %	0.015 / 0.014 %
Vehicle operation cost (C_{sum})	143.49 / 141.00 $	93.78 / 88.74 $

During Test 2, the battery temperature is shown in Figure 17. At the beginning of preheating process, battery temperature failed to rise promptly. This is because the liquid in water cycles needed some time to be heated firstly, and then the battery could be heated by the liquid. In charging process, real battery temperature was a little lower than simulated temperature at first, which was because the temperature was collected on the surface of battery. In simulation, battery was considered as a lumped mass, but the truth was that the heat conduction inside battery was not that fast. In the second half of charging process, battery temperature went down due to that with the charging current fell, battery IHG was not able to compensate the heat dissipated to the ambient. Finally during driving process, both test and simulation showed a similar rising trend in fluctuation. The increase in battery temperature during driving was approximately 8 °C, which also indicated that battery IHG cannot be neglected even for short-distance driving range.

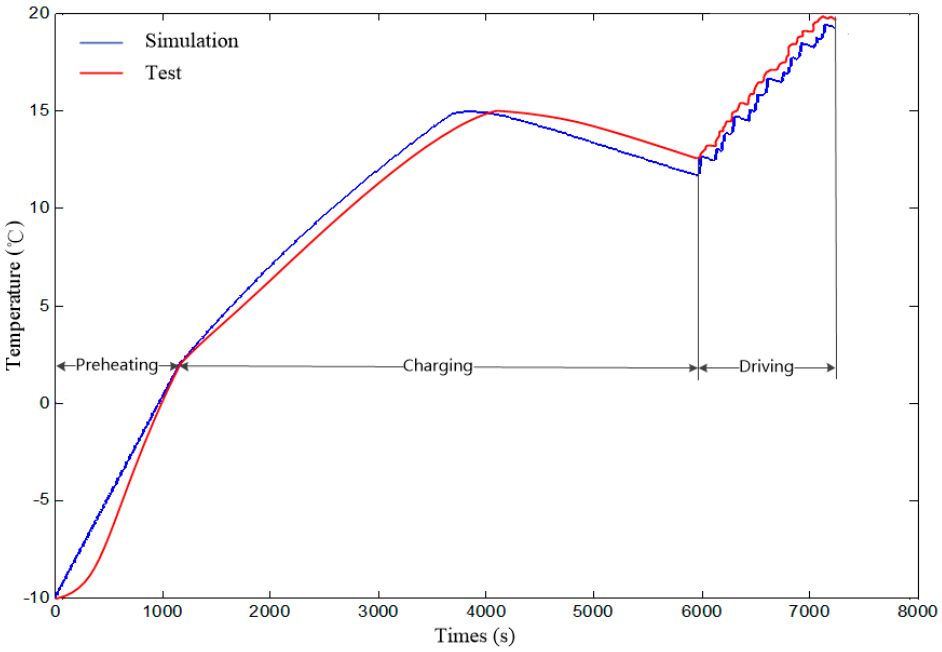

Figure 17. Battery temperature curve during Test 2

7. Conclusion

In conclusion, this paper presents a novel preheating management strategy aiming at lowering total vehicle operation cost. Based on analysis on electro-thermal performance and aging model of LiFePO4 battery, a coupled battery model is proposed. For automotive analysis, vehicle operation cost of electric bus is deduced from two perspectives: electricity consumption cost and battery fade

cost. Under the principle of least vehicle operation cost, optimal preheating target temperatures are determined. A liquid-heating preheating system has also been implemented on an electric bus. Comprehensive simulation results suggest that as ambient temperature declines, preheating process becomes increasingly important to avoid the severe battery capacity degradation at low temperatures, thus the optimal preheating target temperatures grow with decreasing ambient temperatures. On the other hand, rising driving range calls for a descending preheating target temperature, because during vehicle operation battery can heat itself and longer distance running leads to a higher temperature at which battery also suffers a severer degradation. The rationality of this preheating management strategy has been verified by vehicle tests.

For application of this strategy in other situations, it must be highlighted here the optimal preheating target temperatures may shift with different driving cycles, battery types, battery price and efficiency of preheating system. A deficiency in this paper is that the battery is always considered as brand new. But the truth is that battery degradation speed slows down as total Ah-throughput increases. So for used batteries, their degradation speed is slower than that of brand new batteries at same working conditions, consequently lowering optimal preheating target temperatures because of less severe capacity degradation. Fortunately, the optimal preheating target temperatures of used batteries can also be determined by using the methods proposed in this paper, but the precondition is that the total Ah-throughout can be known before optimization.

The long heating time of the implemented heating system also remains to be ameliorated, and because of this, the utilization of vehicle should be well-planned in advance. On the other hand, a good heating system with high efficiency can significantly improve driving economy. Future work will try to improve the heating system with other approaches.

Acknowledgments: The authors gratefully acknowledge the financial support from the National Natural Science Foundation of China (51107052) and the Key Science and Technology Projects of Science and Technology Department of Jilin Province (20150204016GX).

Author Contributions:

T. Z. and H.T. M were responsible for total article structure design and writing; Y.B. Y. contributed the literature review and the funding support; Z.M. Z. and T. X. contributed the implementation of preheating system and vehicle test; Y. C. and X.Y. L. conducted experiments regarding batteries and helped rearranged the paper structure.

Conflicts of Interest:

The authors declare no conflict of interest.

References

1. Doughty, D. H.; Butler, P. C.; Jungst, R. G.; Roth, E. P. Lithium battery thermal models. *J. Power Sources* **2002**, *110*, 357-363.
2. Lee, S.; Kim, J.; Lee, J.; Cho, B. H. State-of-charge and capacity estimation of lithium-ion battery using a new open-circuit voltage versus state-of-charge. *J. Power Sources* **2008**, *185*, 1367-1373.
3. Yang, J.; Cai, S. Battery pack thermal management system and method. U.S. Patent 8658299, Feb. 25, 2011.
4. Lake, B. J.; Ziehr, L.; Tagliapietra, L. C. Controller for heating in reversible air conditioning and heat pump HVAC system for electric vehicles. U.S. Patent 6118099, Sep. 12, 2000.
5. Chakib, A. Electric vehicle energy management system. D. Eng., University of Massachusetts Lowell, USA, 2001.
6. Apfelbeck, R.; Barthel, F.; Heating Comfort and Range Perfectly Combined-Heating Systems for Vehicles with Alternative Drive System. Prospects and Challenges of Biofuel-Operated Water and Air Heaters. In Proceedings of the SAE 2013 World Congress & Exhibition, Detroit, MI, USA, 16-18 April, 2013.
7. Lin, C.; Xu, S.; Li, Z.; Li, B.; Chang, G.; Liu, J.; Thermal analysis of large-capacity LiFePO4 power batteries for electric vehicles. *J. Power Sources* **2015**, *294*, 633-642.
8. Jaguemont, J.; Boulon, L.; Dubé, Y.; A comprehensive review of lithium-ion batteries used in hybrid and electric vehicles at cold temperatures. *Appl. Energy* **2016,** *164*, 99-114.
9. Xu, M.; Zhang, Z.; Wang, X.; Jia, L.; Yang, L. A pseudo three-dimensional electrochemical–thermal model of a prismatic LiFePO4 battery during discharge process. *Energy*, **2015**, *80*, 303-317.

10. Kang, J.; Rizzoni, G.; Study of relationship between temperature and thermal energy, operating conditions as well as environmental factors in large-scale lithium-ion batteries. *Energy Res.* **2014**, *38*, 1994-2002.
11. Agarwal, V.; Uthaichana, K.; Decarlo, R.A.; Tsoukalas, L.H.; Development and Validation of a Battery Model Useful for Discharging and Charging Power Control and Lifetime Estimation. *IEEE Trans. Energy Conv.* **2010**, *25*, 821-835.
12. Ahmed, S. H.; Kang, X.; Shrestha, S. O. B.; Effects of Temperature on Internal Resistances of Lithium-Ion Batteries. *J Energy Resources Technol.* **2015**, *137*, 0195-0738.
13. Bhattacharyya, R.; Key, B.; Chen, H.; Best, A. S.; Hollenkamp, A. F.; Grey, C. P.; In situ NMR observation of the formation of metallic lithium microstructures in lithium batteries. *Nat. Mats.* **2010**, *9*, 504-510.
14. Petzl, M.; Kasper, M.; Danzer, M. A.; Lithium plating in a commercial lithium-ion battery-A low-temperature aging study. *J .Power Sources* **2015,** *275*, 799-807.
15. Kwon, O. J.; Fang, W.; Wang, C.; Lithium Deposition in the Anode of an Automotive Li-Ion Battery: Experiments and Modeling. *Pcs-Pol. Culture & Socialization.***2010,** *1*, 279.
16. Sarasketa-Zabala, E.; Gandiaga, I.; Martinez-Laserna, E.; Rodriguez-Martinez, L. M.; Villarreal, I.; Calendar ageing analysis of a LiFePO4/graphite cell with dynamic model validations: Towards realistic lifetime predictions. *J. Power Sources* **2014**, *275*, 573-587.
17. Groot, J.; Swierczynski, M.; Stan, A. I.; Kær, S. K.; On the complex ageing characteristics of high-power LiFePO4/graphite battery cells cycled with high charge and discharge currents. *J. Power Sources* **2015**, *286*, 475-487.
18. Waldmann, T.; Wilka, M.; Kasper, M.; Fleischhammer, M.; Wohlfahrt-Mehrens, M.; Temperature dependent ageing mechanisms in lithium-ion batteries – A post-mortem study. *J. Power Sources* **2014**, *262*, 129-135.
19. Wang, J.; Liu, P.; Hicks-Garner, J.; Sherman, E.; Soukiazian, S.; Verbrugge, M.; Tataria, H.; Musser, J.; Finamore, P.; Cycle-life model for graphite-LiFePO$_4$ cells. *J. Power Sources* **2011**, *196*, 3942-3948.
20. Wang, J.; Purewal, J.; Liu, P.; Hicks-Garner, J.; Soukazian, S.; Sherman, E.; Sorenson, A.; Vu, L.; Tataria, H.; Verbrugge, M. W.; Degradation of lithium ion batteries employing graphite negatives and nickel-cobalt- manganese oxide + spinel manganese oxide positives: Part 1, aging mechanisms and life estimation. *J. Power Sources* **2014**, *269*, 937-948.
21. Rao, Z.; and Wang, S.; A review of power battery thermal energy management. *Renew. Sustain. Energy Rev.* **2011**, *15*, 4554-4571.
22. Chen, Y.; and Evans, J. W.; Heat transfer phenomena in lithium/polymer-electrolyte batteries for electric vehicle application. *J. Electrochem. Soc.* **1993**, *140*, 1833-1837.
23. Ji, Y.; Wang, C.; Heating strategies for Li-ion batteries operated from subzero temperatures. *Electrochim. Acta*, **2013**, *107*, 664-674.
24. Zhang, J.; Ge, H.; Li, Z.; Ding , Z.; Internal heating of lithium-ion batteries using alternating current based on the heat generation model in frequency domain. *J. Power Sources* **2015**, *273*, 1030-1037.
25. Pesaran, A. A.; Vlahinos, A.; Stuart, T. A.; Cooling and Preheating of Batteries in Hybrid Electric Vehicles. In Proceedings of the 6th ASME-JSME Thermal Engineering Joint Conference, Honolulu, Hawaii, USA, 13-17 March, 2003.
26. Wang, Q.; Jiang, B.; Xue, Q.; Sun, H.; Li, B.; Zou, H.; Yan, Y.; Experimental investigation on EV battery cooling and heating by heat Pipes. *Appl. Therm. Eng.* **2015**, *88*, 54-60.
27. Song, Z.; Hofmann, H.; Li, J.; Hou, J.; Zhang, X.; Ouyang, M.; The optimization of a hybrid energy storage system at subzero temperatures: Energy management strategy design and battery heating requirement analysis. *Appl. Energy* **2015**, *159*, 576–588.
28. Bauer, S.; Suchaneck, A.; León, F. P.; Thermal and energy battery management optimization in electric vehicles using Pontryagin's maximum principle. *J. Power Sources* **2014**, *246*, 808-818.
29. Rao, R.; Virudhula, S.; and Rakhmatov, D.; Battery models for energy aware system design. *Computer* **2003**, *36*, 77-87.
30. Zhe, L.; Han, X.; Lu, L.; Ouyang, M.; Temperature Characteristics of Power LiFePO4 Batteries. *J. Mech. Eng.* **2011**, *47*, 115-120.
31. Gao, H.; Lv, F.; Wei, X.; Dai, H.; Research of Li-ion battery's energy efficiency. *Chinese J. Power Sources* **2013**, *12*, 2132-2134.
32. Bernardi, D.; Pawlikowski, E.; Newman, J.; A general energy balance for battery systems. *J. Electrochem. Soc.* **1985**, *132*, 5-12.
33. Damay, N.; Forgez, C.; Bichat, M. P.; Friedrich, G.; Thermal modeling of large prismatic LiFePO4/graphite battery. Coupled thermal and heat generation models for characterization and simulation. *J. Power Sources* **2015**, *283*, 37-45.

34. Johnson V. H.; Battery performance models in ADVISOR. *J. Power Sources* **2002**, 110, 321–329.
35. Bandhauer, T. M.; Garimella, S.; Fuller, T.; A Critical Review of Thermal Issues in Lithium-Ion Batteries. *J. Electrochem. Soc.* **2011**, *158*, 1-25.
36. Pesaran, A.; Keyser, M.; Burch, S.; An approach for designing thermal management systems for electric and hybrid vehicle battery packs. In Proceedings of the 1999 Vehicle Thermal Management Systems Conference, London, England, Jan. 1999.
37. Hallaj, S. A.; Maleki, H.; Hong, J. S.; Selman, J. R.; Thermal modeling and design considerations of lithium-ion batteries. *J. Power Sources* **1999**, *83*, 1-8.
38. Steffke, K. W.; Spigno, C.; Bezzina, C.; Li-ion Air-Cooled Battery System Interactions with the Vehicle HVAC System. In Proceedings of the SAE 2013 World Congress & Exhibition, Detroit, MI, USA, 16-18 April, 2013.
39. Jaguemont, J.; Boulon, L.; Venet, P.; Dube, Y.; Lithium-Ion Battery Aging Experiments at Subzero Temperatures and Model Development for Capacity Fade Estimation. *IEEE Trans. Vehar. Technol.* **2016**, *65*, 4328-4343.
40. Ehsani, M.; Gao, Y.; Emadi, A.; *Modern Electric, Hybrid Electric, and Fuel Cell Vehicles Fundamentals, Theory, and Design*, 2nd ed.; CRC Press, Boca Raton, FL, USA, 2010; pp 89-362.
41. Deb, K.; Pratap, A.; Agarwal, S.; Meyarivan, T.; A Fast and Elitist Multi-objective Genetic Algorithm: NSGA-II. *IEEE Trans. Evolut. Comput.* **2002**, *6*,182-197.
42. Qin, Z.; Wang, J.; Li, J.; Study on the Special Thermal Management System of Extended-range EV. *Auto Elec. Parts* **2013**, *12*, 5-8.
43. Yokoyama, A.; Osaka, T.; Imanishi, Y.; Sekiya, S.; Thermal management system for electric vehicles. *SAE Int. J. Mats. & Manuf.* **2011**, *4*, 1277-1285.
44. Zheng, Y.; Ouyang, M.; Lu, L.; Li, J.; Understanding aging mechanisms in lithium-ion battery packs: From cell capacity loss to pack capacity evolution. *J. Power Sources* **2015**, *278*, 287-295.